ELSEVIER

Ceramics International 33 (2007) 579–587

CERAMICS INTERNATIONAL

www.elsevier.com/locate/ceramint

Effect of Ca-additions on structural and electrical properties of $Pb(SnTi)O_3$ nano-ceramics

Shrabanee Sen [a,*], P. Pramanik [b], R.N.P. Choudhary [a]

[a] *Department of Physics and Meteorology, Indian Institute of Technology, Kharagpur 721302, India*
[b] *Department of Chemistry, IIT Kharagpur, Kharagpur 721302, India*

Received 11 April 2005; received in revised form 9 September 2005; accepted 26 November 2005
Available online 14 February 2006

Abstract

Polycrystalline samples of Ca-modified $Pb(SnTi)O_3$ (i.e., $Pb_{1-x}Ca_xSn_{0.15}Ti_{0.85}O_3$, $x = 0$, 0.03, 0.06 and 0.09) were prepared by the precursor solution method. X-ray diffraction (XRD) of the compounds suggests that they exhibit single phase with tetragonal crystal structure. SEM micrograph of the materials shows uniform grain distribution on the surface of the samples. TEM micrographs of the above compounds reveal that their particle size is less than 30 nm. Detailed dielectric studies of the compounds at different temperature suggest that with increasing Ca concentration in the compound, the value of the dielectric constant first increases for ($x = 0$, 0.03 and 0.06) and then decreases for ($x = 0.09$). The compounds do not exhibit any ferroelectric relaxor behavior, i.e., they exhibit diffuse phase transition and frequency dependent high permittivity. Some impedance and electrical properties of the materials were studied using an impedance spectroscopic technique (CIS) in a wide range of temperature (30–500 °C). The Nyquist plot clearly shows the presence of both bulk and grain boundary effects in all the compounds.

Keywords: C. Electrical conductivity; Ceramics; X-ray diffraction; Impedance spectroscopy

1. Introduction

Since the discovery of ferroelectric properties in barium titanate and lead titanate a large number of titanate and doped/modified compounds described by the general formula ABO_3 (A = monovalent, B = tri/hexavalent ions) have been studied for solid state devices. Titanates have been studied since last century, due to their eminent properties such as dielectric [1], ferroelectric [2], piezoelectric [3] and pyroelectric properties [4]. The selection of dopants to tailor the physical properties of the materials is based on many factors including (a) charge neutrality, (b) tolerance factor (t) where t is defined as $t = (r_A + r_o)/\sqrt{2}(r_B + r_o)$ where r_A and r_B are the average radius of A and B site ions, respectively, and r_o is the ionic radius of oxygen, (c) ionic radius and (d) solubility/miscibility [5,6]. It is clearly concluded from the phase diagram of $PbTiO_3$–$PbSnO_3$ that $Pb(SnTi)O_3$ solid solution (PST) can be prepared in various crystal systems. Literature survey shows that PST in different Sn/Ti ratios [7] has provided many interesting properties. It has also been reported that a higher percentage of Sn (>80%) in PST does not show a perovskite phase with ferroelectric properties. Therefore, we have studied the structural and electrical properties of Ca-modified PST, with small concentration of Sn (up to 15%). The impedance spectroscopy technique has been used to separate the grain and grain boundary effect.

2. Experimental procedure

Polycrystalline PCST compounds were synthesized by a solution based chemical method, which is less cumbersome, more versatile and cost effective. This technique begins with the preparation of a precursor solution in which the ions are well dispersed on a molecular scale along with organic compounds. A careful control of the removal of the organic matrix provides the production of ultrafine (nanosized) powder without agglomeration.

Fine powders of the compounds were prepared using high purity raw materials: $Pb(NO_3)_2$, $Ca(NO_3)_2$, SnC_2O_4-solution, EDTA, TEA, and titanium tartarate. As some of the metal complexes (tin oxalate (SnC_2O_4) and titanium tartarate) were not commercially available, these were first prepared in the form of solution in our laboratory as follows.

* Corresponding author.
E-mail address: sraban@phy.iitkgp.ernet.in (S. Sen).

0272-8842/$32.00
doi:10.1016/j.ceramint.2005.11.007

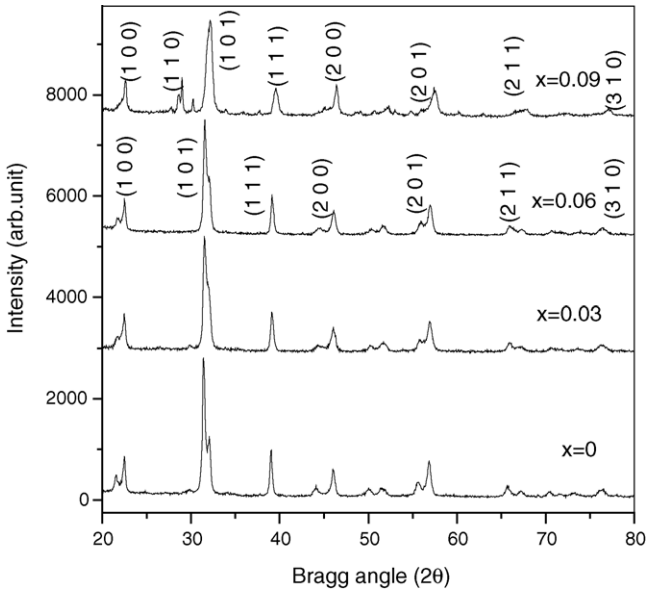

Fig. 1. XRD pattern of PCST ($x = 0$, 0.03, 0.06 and 0.09) compounds.

Titanium tartarate was prepared by dissolving titanium oxide (Aldrich, 98%) in HF (Merck, 40% solution) (1:7 mole ratio) and keeping the mixture in a water bath for 72 h. A clear solution of titanium fluoro-complex was produced. Addition of dilute ammonia to that clear solution resulted in the formation of insoluble hydrous titanium hydroxide (TiO_2, nH_2O). The respective hydrous oxide was then separated from the solutions by filtration and was repeatedly washed with 5% ammonia solution to yield hydrous titanium oxide free from chloride ions. After estimating the amount of TiO_2 present in $TiO_2{\cdot}nH_2O$ by heating a small amount of it at 1000 °C for 2 h, the hydrous TiO_2 was dissolved in tartaric acid (Quest, 99%) (1:4 mol) with constant stirring at 60 °C for about 8 h to obtain titanium tartarate.

Table 1
Comparison of lattice parameters (a and c in Å) with the standard deviation of ±0.0012 Å, volume V (in Å), the crystallite size (P) in nm and density (D) in g/cm^3 of PCST ($x = 0$, 0.03, 0.06 and 0.09) compounds

x	a	c	V	P (XRD)	P (TEM)	D
0	4.0283	4.0072	65.02	18	22	3.63
0.03	4.0140	4.0039	64.34	16	27	3.56
0.06	4.0128	3.9953	64.33	14	19	4.01
0.09	3.9975	3.8824	62.04	20	25	3.98

Stannous oxalate (SnC_2O_4) was prepared by mixing aqueous solution of stannous chloride ions (Merck, 95%), ammonium oxalate (SRL, 99%) and oxalic acid (SRL, 99.5%) in 1:1:1 mole ratio. The mixture was then kept in water bath for 2 h, resulting in a white stannous oxalate residue. Clear aqueous solution of stannous oxalate was obtained by treating it with ammonical aqueous solution of nitrilotriacetic acid (Loba, 99%) (1:1 mol) at pH 5. The pH of the solution was adjusted using dilute ammonia and formic acid solution. Lead nitrate ($Pb(NO_3)_2$) (BDH, 99%) (excess 1%) was added to ammonical solution of ethylenediaminetetracetic acid (EDTA) (SRL 99%) in 1:1 ratio in order to form Pb–EDTA complex and then required amount of calcium nitrate ($Ca(NO_3)_2$) (BDH, 99%)

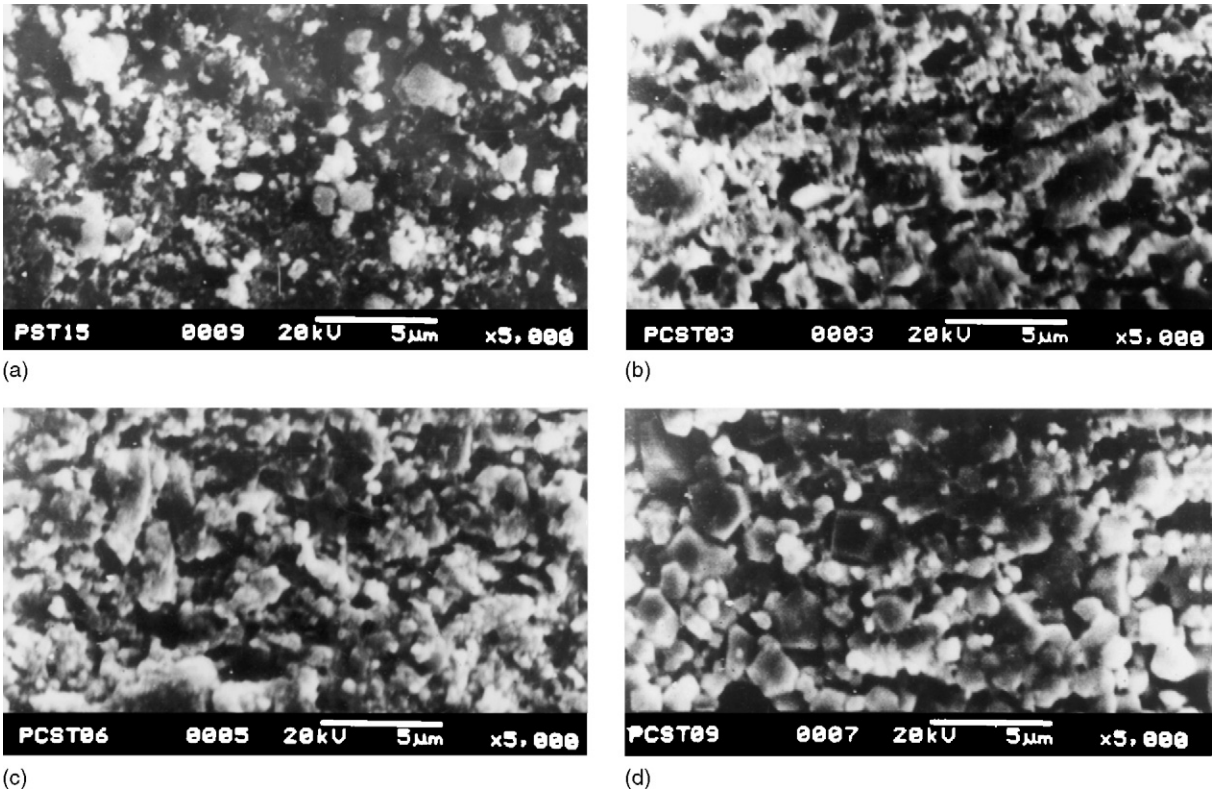

Fig. 2. SEM micrographs of PCST ($x = 0$, 0.03, 0.06 and 0.09) compounds.

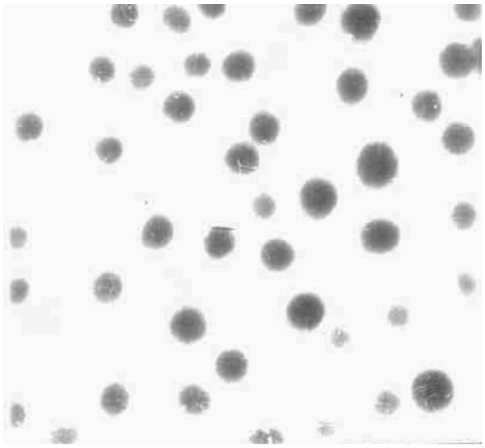

(a)

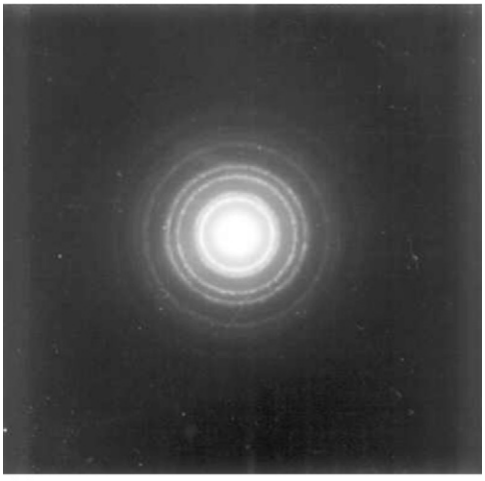

(b)

Fig. 3. (a) TEM micrograph of PCST ($x = 0$) compound. (b) Corresponding SAED patterns.

was added to it to get Pb-EDTA and Ca-EDTA complex. EDTA acts as hexadentate ligand in which, if any metal ion is added, it forms a negatively charged metal complex, which prevents the possibility of precipitation of the metal ions. Stoichiometric amount of Pb-EDTA, Ca-EDTA, Sn-oxalate and Ti-tartarate were mixed followed by addition of triethleyene amine (TEA) (Merck, >97%) (5 mol of the total metal ion) resulting in a clear precursor solution. The complexing agents helps to keep the metal ions uniformly distributed throughout the solution at the time of evaporation without undergoing precipitation or segregation of the cations from the solution. Also, the carbonaceous material generated from the complete evaporation of the complexing agents provides heat through combustion and facilitates the reaction at reduced external temperature to get the desired fine powders. A fluffy, mesoporous-carbon rich precursor mass was formed by complete evaporation of the precursor solution by heating it at 200 °C. This was due to the decomposition of the metal complexes, EDTA and TEA with simultaneous evolution of dense fumes. The voluminous, fluffy black carbonaceous mass was heated at 800 °C for 4 h to produce the desired compounds in single phase which was confirmed by X-ray diffraction using Cu Kα target ($\lambda = 1.5418$ Å) for a wide range of Bragg angles 2θ ($20^\circ \leq 2\theta \leq 80^\circ$) at a scanning rate of 2°/min. The calcined powder was then used to make cylindrical pellets of 10 mm diameter and a thickness of 1–2 mm using a hydraulic press at a pressure of 6×10^7 N/m^2. Polyvinyl alcohol (PVA) was used as a binder to reduce the brittleness of the pellets. The pellets were sintered at 1000 °C for 10 h in air. In order to prevent lead loss (from the pellets) during sintering at high temperature, the pellets were covered by lead zirconate. The sintered unpolished flat surface of the pellet was gold coated by sputtering in order to study the surface morphology of the pellets. The surface morphology of the pellets was studied by means of a scanning electron microscope (JEOL JSM-5800). To investigate the quality of the samples and to estimate the particle size more accurately, selected area diffraction patterns (SAED) were taken by transmission electron microscopy (HITACHI-H 600).

In order to study the electrical properties, both the flat surfaces of the samples were polished and covered with high purity silver paint. All the silver painted samples were dried at 180 °C for 4 h to remove moisture, if any. The electrical measurements were carried out using a computer controlled impedance analyzer (HIOKI 3532 LCR HITESTER) in the frequency range of 100 Hz–1 MHz.

3. Results and discussion

3.1. Structure and microstructure

The formation of single-phase compounds was checked by studying some aspects of structural analysis by X-ray diffraction (XRD). The XRD patterns of all the four compounds $Pb_{1-x}Ca_xSn_{0.15}Ti_{0.85}O_3$ (PCST with $x = 0$, 0.03, 0.06 and 0.09) are shown in Fig. 1. This involves a reconstructive molecular decomposition and spontaneous combustion of polymer precursor from a high energy amorphous state [8]. As a consequence controlled nucleation growth of nanoparticles has taken place at this temperature. All the reflection peaks were indexed and the lattice parameters were determined in various crystal systems using a computer program package ''powdmult'' [9]. On the basis of the best agreement between calculated (cal) and observed (obs) interplanar d-spacings (d_{obs} and d_{cal}), a suitable unit cell of the compounds in the tetragonal system was selected. The lattice parameters were refined by least-squares fitting technique. The refined lattice parameters are given in Table 1. The crystallite size was estimated from the broadening of reflection peaks using the Scherrer's equation, $P = 0.89\lambda/\beta_{1/2}\cos\theta$ [10,11] where $\beta_{1/2}$ is the half peak width. Since powder samples were used in taking XRD pattern, the broadening due to mechanical strain and instrument errors was ignored.

The SEM micrographs of the sintered pellets are shown in Fig. 2. The addition of excess Pb during sintering enhances the densification of pellets. It leads to a liquid phase formation on the grain boundaries in the initial stage of sintering, and thus promotes a rapid densification process. This effect decreases the residual porosity that occurs on microstructure. It is observed that the shape of the grains been changed with the increasing doping Ca concentration in PCST. Thus, doping has produced significant effect on the microstructure of the samples.

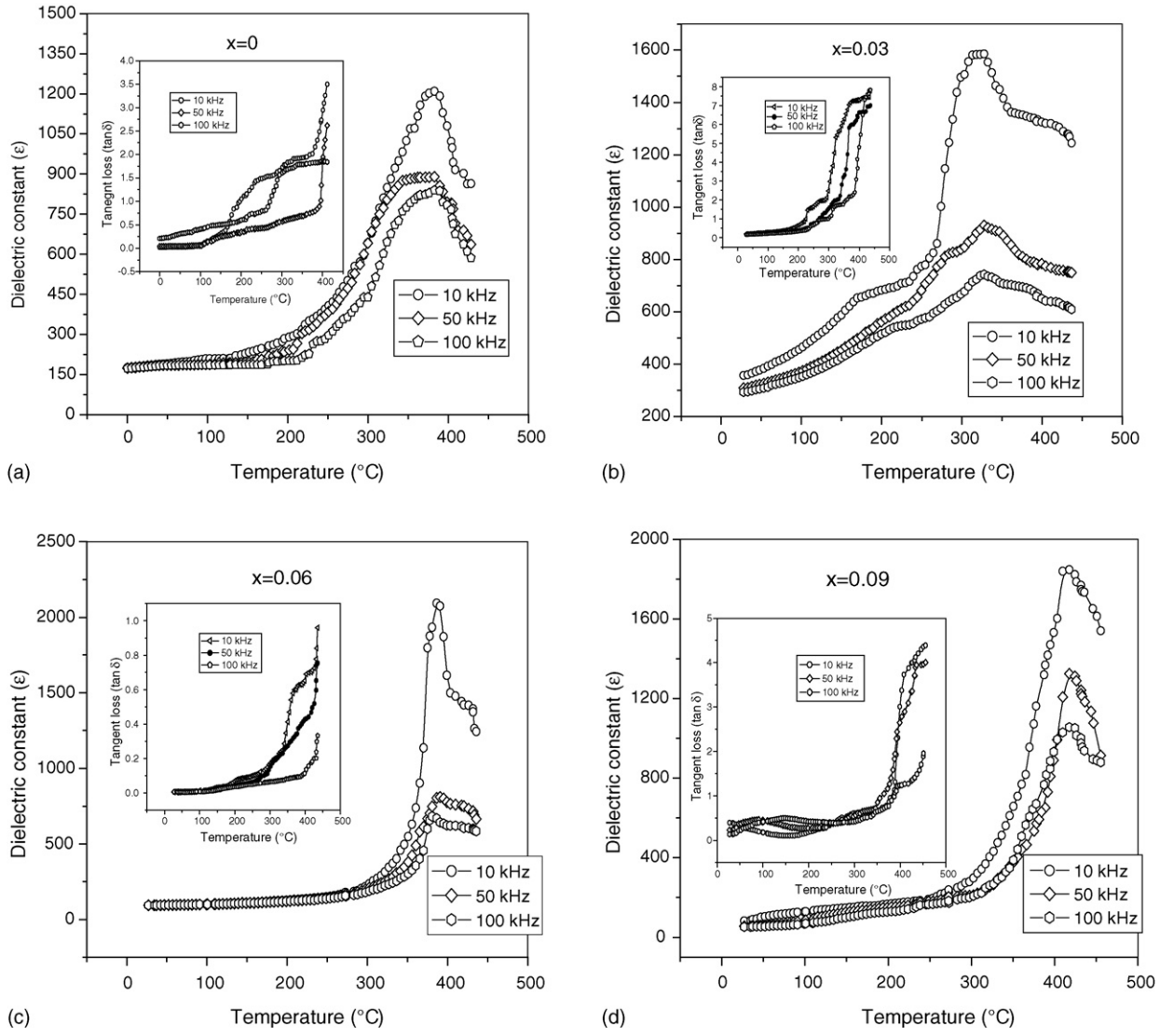

Fig. 4. Plot of variation of dielectric constant and tangent loss of PCST ($x = 0$, 0.03, 0.06 and 0.09) compounds.

The TEM micrographs along with the SAED patterns are shown in Fig. 3. The small spots can be identified as particle/crystallite agglomerates. The particles are spherical in shape, with average diameter of 20–30 nm. The corresponding selected area electron diffraction of the samples was taken some of which showed distinct rings (Fig. 3(b)), which are the characteristics of assembly of crystallite/particle agglomerate. The particle size calculated from TEM micrographs are given in Table 1. It is seen that the crystallite size calculated from TEM micrographs is larger than the calculated one using Scherrer's equation, due to the obvious fact that all the errors are not eliminated while calculating the crystallite size.

3.2. Electrical properties

3.2.1. Dielectric properties

The temperature variation of dielectric constant of all the Ca doped PST compounds is shown in Fig. 4. It has been noticed that the transition temperature shifts towards higher temperatures and that the value of the dielectric constant first increases with increasing Ca concentration (up to 6%) but decreases (for 9% Ca-doped) in PST compounds. These compounds undergo a phase transition from the ferroelectric to the paraelectric state at 382, 318, 386 and 414 °C for $x = 0$, 0.03, 0.06 and 0.09, respectively. This change may be related to several factors such as (1) effect of doping, (2) domain reorientation and (3) stress boundary condition on the individual crystallites [12]. For all the frequencies 10, 50 and 100 kHz the dielectric constant (ε) reaches a maximum at the same Curie temperature and the value of ε at the transition temperature are 1210, 1583, 2093 and 1863 for $x = 0$, 0.03, 0.06 and 0.09, respectively. The compounds do not show frequency dispersion and hence exhibit non-relaxor property, which means that there is no shift in the transition temperature with frequency.

The temperature variation of the tangent loss of all the Ca doped PST compounds are shown in Fig. 3. The sharp rise in tan δ may be due to the scattering of thermally activated charge carriers and some defects in the samples. At higher temperature the conductivity begins to dominate, which in turn responsible for the rise in tan δ (i.e., $\sigma \propto \tan \delta$). At high temperature

(paraelectric phase) the contribution of ferroelctric domain walls to tan δ decreases, which is also responsible factor for the rise in tan δ at high temperature [13].

3.2.2. Impedance analysis

Impedance spectroscopy is a useful technique to analyze the electrical properties of low conductivity materials and electroceramics [14]. It helps in determining the relaxation frequency and separation of grain and grain boundary effects. This is particularly relevant for polycrystalline ferroelectric materials in which the temperature-dependent variation of the capacitance associated with the ferroelectric component explains high value of the dielectric constant at Curie temperature with Curie–Weiss decay above it. A polycrystalline material usually presents grain and grain boundary properties with different time constants leading to two successive semicircles. The second intercept of the high frequency semicircle with the real axis is the bulk resistance (R_b) of the sample. The electrical properties are often represented in terms of some complex parameters like complex dielectric constant (ε^*), complex impedance (Z^*), electric modulus (M^*) and tangent loss (tan δ). They are related to each other as $Z^* = Z' - jZ'' = R_S - 1/j\omega C_s$, $\varepsilon^* = \varepsilon' - j\varepsilon''$, $M^* = M' + jM'' = j\omega\varepsilon_o Z^*$, $\tan\delta = \varepsilon''/\varepsilon'$ where ε_o is the permittivity in free space, R_s and C_s are the resistance and capacitance in series and $j = \sqrt{-1}$ is the imaginary operator. The above four expressions offer a wide scope for graphical representation. In all ferroelectrics, in general the study of electrical conductivity that is calculated from impedance formalism since the associated physical properties like piezoelectricity, pyroelectricity are dependent on the order and nature of conductivity in the materials [15]. The plot of Z' with Z'' at various temperature is shown in Fig. 5. The presences of two semicircles in all the plots show the presence of both bulk

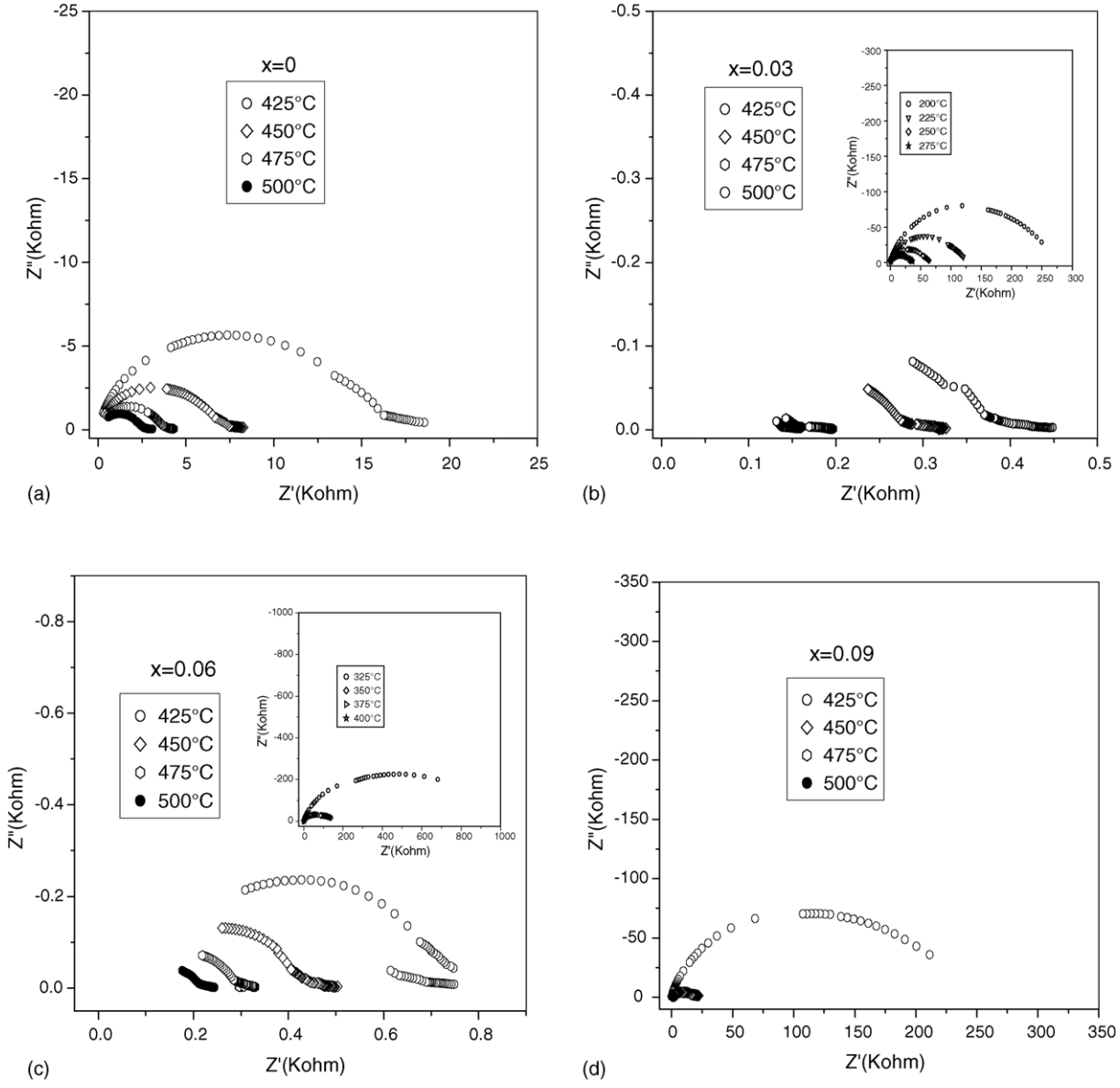

Fig. 5. Plot of real part of impedance (Z') with imaginary part of impedance (Z'') of PCST ($x = 0$, 0.03, 0.06 and 0.09) compounds.

property and non-homogeneous electrical behavior of grain boundaries. Each semicircle is represented by a parallel RC circuit that corresponds to individual components of the material. The variation of real part of impedance (Z') with frequency at different temperature and various concentration of Ca is shown in Fig. 6. The magnitude of Z' decreases on increasing temperature, which indicates the increase in a.c. conductivity. Large value of Z' at low frequency and temperature clearly shows the effect of polarization in the samples under present study. At higher frequency the value of Z' merges for all temperature for PCST ($x = 0$ and 0.09) ions which clearly indicates the presence of space charge polarization [16] due to which there must be a reduction in the barrier properties of the material with rise in temperature and this may be a responsible factor for the enhancement of a.c. conductivity of the material with temperature at higher frequencies. The nature of the curves implies that complex impedance of electrode-material-electrode capacitor could be demonstrated as the sum of the single RC circuit with parallel combination [17]. Therefore,

$$Z^*(T) = Z_0(T) \int_0^\infty \frac{y(\tau, T)\mathrm{d}(\tau)}{1 + j\omega\tau}$$

which gives:

$$Z'(\omega, T) = Z_0(T) \int_0^\infty \frac{y(\tau, T)\mathrm{d}(\tau)}{1 + \omega^2\tau^2}$$

$$Z''(\omega, T) = Z_0(T) \int_0^\infty \frac{(\omega\tau)^* y(\tau, T)\mathrm{d}(\tau)}{1 + \omega^2\tau^2}$$

where $\tau = RC$, relaxation time. $y(\tau, T)$ determines the distribution of relaxation times. In case of a broad spectrum

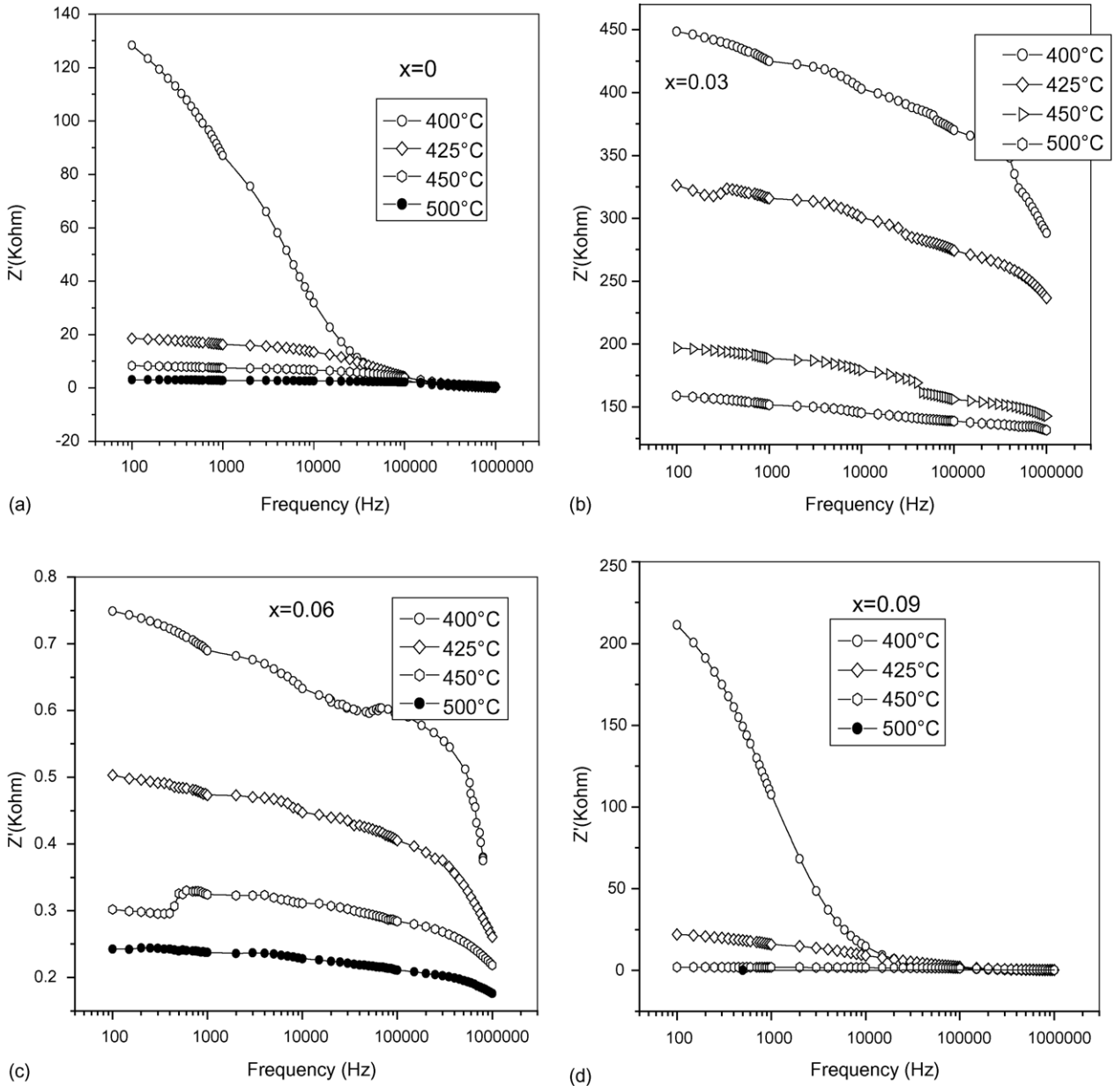

Fig. 6. Plot of real part of impedance (Z') with frequency of PCST ($x = 0$, 0.03, 0.06 and 0.09) compounds.

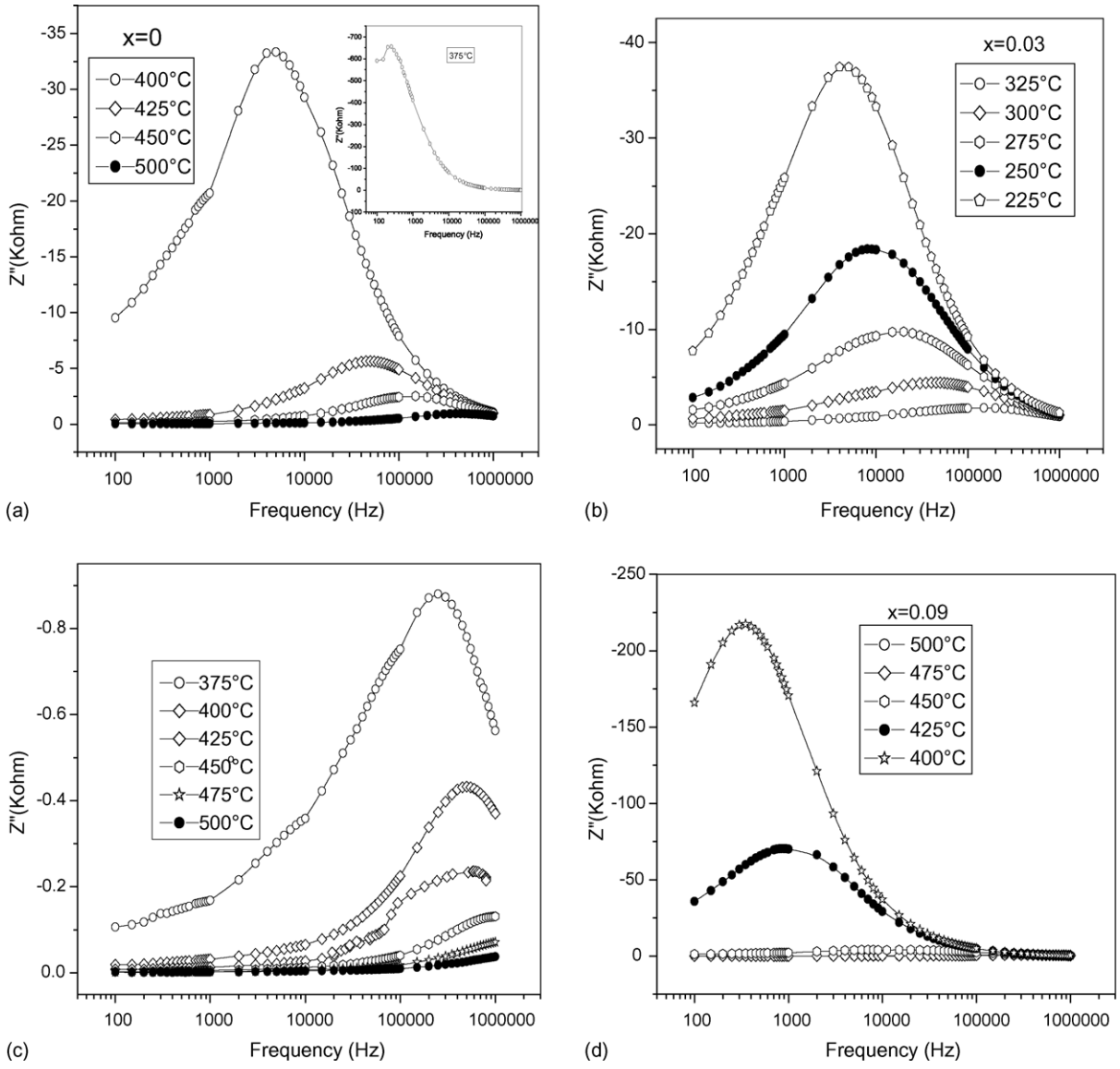

Fig. 7. Plot of imaginary part of impedance (Z'') with frequency of PCST ($x = 0$, 0.03, 0.06 and 0.09) compounds.

(i.e., $\tau_{min} \leq \tau \leq \tau_{max}$), Z'' could be approximated as discussed by others [18]: $Z''(\omega, T) \cong KZ_0(T)y(\tau, T)$ where K is a constant.

Fig. 7 provides a plot of the imaginary part of impedance (Z'') with frequency. This representation is most suitable to evaluate the relaxation frequency, which provides an indication about the presence of space charge polarization. There was a clear dispersion of the resultant curves in the low frequency region at different temperature, which merges at higher frequency irrespective of temperature in the entire sample. The broadening of peaks suggests that there is a spread of relaxation times, involving more than two equilibrium positions. The significant broadening of peaks on increasing temperature suggests the presence of a temperature-dependent relaxation process in the materials. The relaxation process may be due to the presence of electrons/immobile species at low temperature and defects at higher temperature [19]. The a.c. conductivity was calculated using the relation $\sigma_{ac} = \omega\varepsilon\varepsilon_o \tan\delta$, where ω is the angular frequency, tan δ is the dissipation factor, ε is the relative dielectric constant and ε_o is the permitivitty in free space.

The plot of a.c. conductivity with different frequencies for all the compounds is shown in Fig. 8. The power law dependence of a.c. conductivity is of a universal nature and corresponds to a short range hopping of charge carriers through trap sites separated by energy barriers of varied heights. Each pair of potential well corresponds to a certain time constant of transition from one site to another. The conductivity $\sigma(\omega)$ can be written as $\sigma(\omega) = \sigma_{dc} + A\omega^n$ known as Jonscher's power law [20] where n is the frequency exponent in the range of $0 \leq n \leq 1$. According to Jonscher, the origin of frequency dependence of conductivity lies in the relaxation phenomena arising due to mobile charge carriers. The low frequency dispersion has been attributed to the a.c.

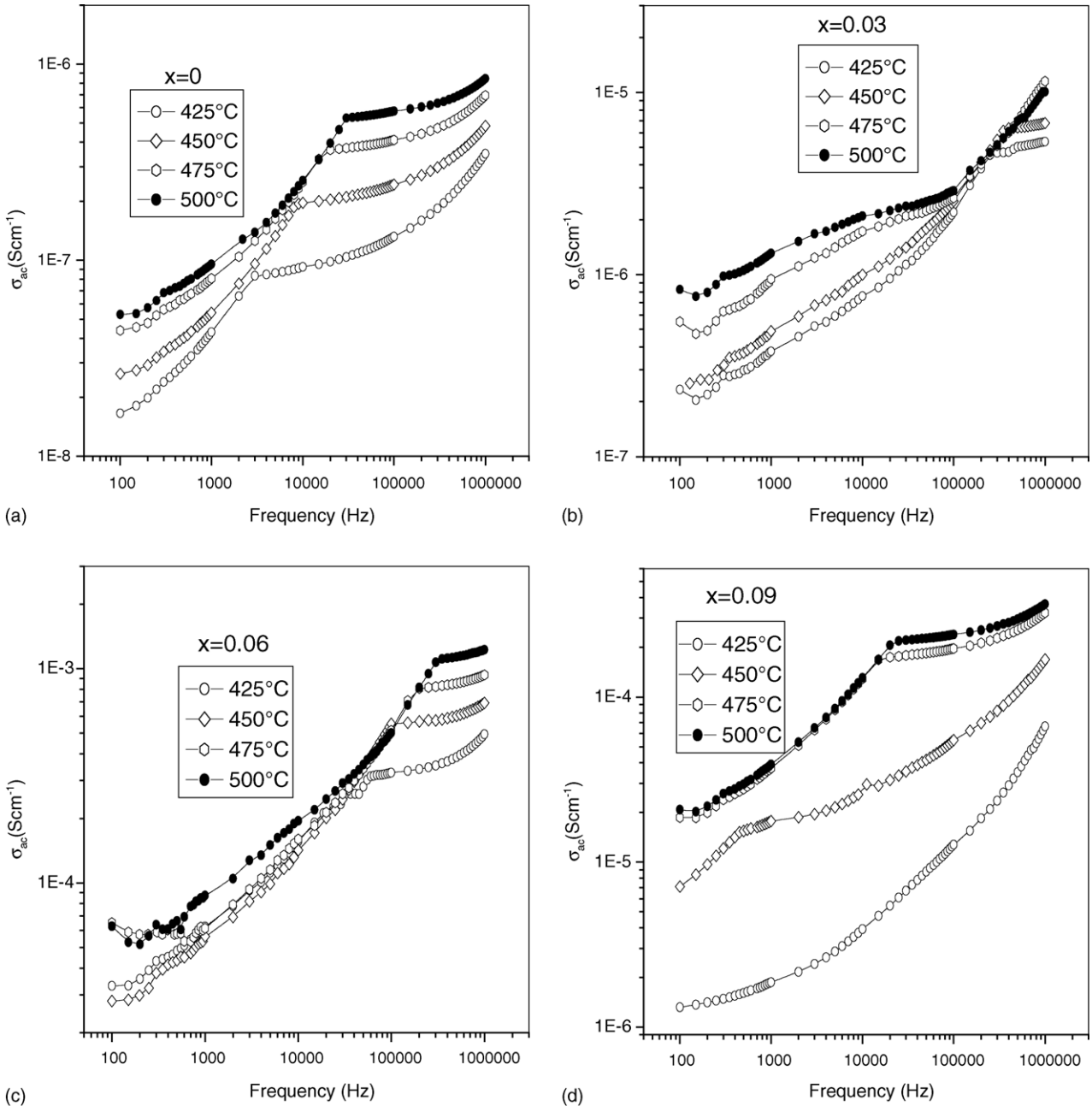

Fig. 8. Plot of a.c. conductivity with frequency of PCST ($x = 0$, 0.03, 0.06 and 0.09) compounds.

conductivity whereas the frequency independent plateau region in he conductivity pattern corresponds to the d.c. conductivity of the materials sample. The temperature at which the grain resistance dominates over grain boundary resistance is marked by a change in slope of a.c. conductivity with frequency. The frequency at which the slope change takes place is known as the hopping frequency, which corresponds to polaron hopping of charged species [21]. The hopping frequency shifts to higher frequency side with temperature. The charged species that have been accumulated at the grain boundaries have sufficient energy to jump over the barrier with increasing temperature and hence increase the conductivity.

4. Conclusion

The nanosized powders were prepared by calcination of precursors obtained after complete dehydration of a solution comprising the ions complexed with TEA and EDTA. The low temperature exothermic decomposition of the organic based precursor materials resulted in high local temperatures, facilitating a solid–solid phase reaction between constituent ions and resulting in the formation of single-phase material at relatively low temperature. Studies of the electrical behavior for all the four compounds using complex impedance analysis (CIS) provide the presence of both bulk and grain boundary effects. A temperature-dependent relaxation phenomenon was

also clearly observed. The compounds exhibit a negative temperature coefficient of resistance (NTCR) behavior.

Acknowledgement

The author (Miss S. Sen) would like to sincerely thank CSIR for the financial assistance.

References

[1] A. Garg, D.C. Agarwal, Effect of rare earth (Er, Gd, Eu, Nd and La) and bismuth additives on the mechanical and piezoelectric properties of lead zirconate titanate ceramics, Mater. Sci. Eng. B 86 (2001) 134.
[2] M. Senthil Kumar, R.R. Sumathi, N.V. Giridharan, R. Jayavel, J. Kumar, Investigation on Al/$BaTiO_3$/GaN MFS structure, Mater. Lett. 52 (2002) 95–98.
[3] Yasuda, H. Ohwa, M. Kume, K. Hayashi, Y. Hosono, Y. Yamashita, Crystal growth and electrical properties of lead indium niobate lead titanate binary single crystal, J. Cryst. Growth 229 (2001) 299–305.
[4] S. Dorfman, D. Fuks, A. Gordon, E. Kotomin, P. Wyder, Some nonlinear properties of ferroelectric smart materials, Phys. B. Condens. Mater. 304 (2001) 339–343.
[5] R.C. Buchanan, Ceramic Materials for Electronics, Marcel Dekker, New York, 1986, pp. 174–225.
[6] L.C. Sengupta, S. Stowell, E. Ngo, M.E. Day, R. Lancio, Barium strontium titanate and non ferroelectric oxide ceramic composite for use in phased array antennas, Int. Ferroelectric 8 (1995) 77–88.
[7] F. Calderon, J.N. Siqueiros, J. Portellos, J.L. Heiras, Diffuse phase transition in (Na, Bi) doped $PbSn_xTi_{1-x}O_3$ ferroelectric ceramics, Solid State Commun. 112 (1999) 219–221.
[8] R.N. Das, P. Pramanik, Low temperature chemical synthesis of nanosized ceramic powder, Br. Ceram. Trans. 99 (2000) 153–156.
[9] POWD, an interactive powder diffraction interpretation and indexing program, Ver 2.1, School of Physical Sciences, Finder's University of South Australia, Bedford Park.
[10] L.B. Alexander, X-ray Diffraction Procedures, Wiles, New York, 1974.
[11] B.D. Cullity, Elements of X-Ray Diffraction Addison, Weisley Publishing Company, Inc, Philippines, 1978, p. 284.
[12] N.K. Singh, R.N.P. Choudhary, A. Panigrahi, Diffuse phase transition in $Ba_5YTi_{3-x}Zr_xNb_7O_{30}$ ferroelectrics, Mat. Chem. Phys. 74 (2002) 113–117.
[13] W. Shockley, W.T. Read, Statistics of the recombination of holes and electrons, Phys. Rev. B 87 (1952) 835.
[14] J. Suchanicz, The low-frequency dielectric relaxation $Na_{0.5}Bi_{0.5}TiO_3$ ceramics, Mat. Sci. Eng. B. 55 (1998) 114–118.
[15] M.E. Lines, A.M. Glass, Principles and Applications of Ferroelectric and Related Materials, Clarendon Press, Oxford, 1977.
[16] A.K. Jonscher, The 'universal' dielectric response, Nature 267 (1977) 673.
[17] M. Vijayakumar, S. Selvasekarapandian, M.S. Bhuvaneswari, G. Hirankumar, G. Ramprasad, R. Subramanian, P.C. Angelo, Synthesis and ion dynamics studies of nanocrystalline Mg stabilized zirconia, Physica B 334 (2003) 390.
[18] K. Funke, Jump relaxation in solid electrolytes, Prog. Solid State Chem. 22 (1993) 111.
[19] A. Laha, S.B. Krupanidhi, Study of relaxor like behavior of laser ablated (Pb, La) TiO_3 thin films, Solid State Commun. 127 (2003) 247.
[20] S. Dutta, S. Bhattacharya, D.C. Agarwal, Electrical properties of ZrO_2-Gd_2O_3 ceramics, Mat. Sci. Eng. B 100 (2003) 191.
[21] Y. Li, M. Liu, J. Gong, Y. Chen, Z. Tang, Z. Zhang, Grain boundary effect in zirconia stabilized with yttria and calcia by electrical measurements, Mat. Sci. Eng. B 103 (2003) 108.